Metals **2012**, *2*, 122-135; doi:10.3390/met2020122

OPEN ACCESS

metals

ISSN 2075-4701
www.mdpi.com/journal/metals/

Article

Characterisation and Mechanical Testing of Open Cell Al Foams Manufactured by Molten Metal Infiltration of Porous Salt Bead Preforms: Effect of Bead Size

Appichart Jinnapat and Andrew Kennedy *

Manufacturing Research Division, Faculty of Engineering, University of Nottingham, Nottingham NG7 2RD, UK; E-Mail: emxaj@nottingham.ac.uk

* Author to whom correspondence should be addressed; E-Mail: andrew.kennedy@nottingham.ac.uk; Tel.: +44-115-9513744.

Received: 16 April 2012; in revised form: 17 May 2012 / Accepted: 28 May 2012 / Published: 1 June 2012

Abstract: Preforms made from porous salt beads with different diameters (0.5–1.0, 1.4–2.0 and 2.5–3.1 mm) have been infiltrated with molten Al to produce porous structures using pressure-assisted vacuum investment casting. Infiltration was incomplete for preforms with high densities. At higher infiltration pressures, penetration of molten Al occurred into beads of all sizes and was predicted using a simple model. The yield strength of the porous structures increased with increasing density and decreasing pore (bead) size. Despite the non-optimum distribution of metal in the porous structure, due to partial infiltration within the beads, the magnitude and density dependence of the yield stress were comparable with those for pure Al foams reported in similar studies. The structural efficiency was improved for structures produced at lower infiltration pressure, where the metal is predominantly distributed in the cell walls. The rate of salt dissolution from the preforms was high, in particular for high density preforms, large beads and preforms infiltrated at low pressures, owing to the ability of the porous beads to collapse as well as dissolve.

Keywords: porous metals; aluminium; liquid metal infiltration; mechanical testing

---

1. Introduction

Porous metals with open, connected cells are ideally suited to applications involving heat exchange with a fluid which permeates the porous structure. The fraction of solid and the size of the pores in the porous metal component are important not only for the thermal performance, but also the flow behaviour of the fluid through it. For a given application, the structure of the porous metal must be optimized to maximize its performance.

Infiltration processing offers a versatile and economical route to the production of porous metal structures, where simple equipment is used and net shape can be obtained [1]. To do so involves four steps: preparation of the leachable preform (usually NaCl for infiltration with Al); infiltration of molten metal into the preform; solidification of the molten metal; and dissolution of the preform in a solvent or water. The relative density of the foam can be controlled by varying the degree of densification of the preform, most commonly by a combination of mechanical pressing and sintering, where the resulting preform volume fraction is in the range of 0.64 to 0.9 [2]. The pore size is dictated by the size of the leachable material.

Porous metals have been made using spherical space holders, manufactured by melting and in-flight spheriodisation techniques [3] or by forming a paste made from fine salt particles mixed with flour and water [4]. Porous metals with spherical pores have been found to be stronger and stiffer than their counterparts with angular pores and this is especially marked for porous structures with small (75 μm) pores. These structures with small pores are also significantly stronger than their counterparts with large (400 μm) pores [2,3]. This difference in strength could not be completely accounted for by the change in topology [2] and has been attributed to the formation of a hard, 100 nm thick, load-bearing oxide layer on the cell surfaces during the salt leaching process. This oxide layer affects plastic flow in the cell walls, the effect being marked for pore sizes below roughly 100 μm [5].

Previous studies by the authors [6,7] presented a process for the manufacture of porous spherical beads by the disintegration, in oil, of a salt paste comprising fine salt powder, flour and water. The work demonstrated how they can be used in the production of porous Al structures with a range of solid fractions. Although only demonstrated for one bead size, the benefits of using porous beads included the ability to infiltrate the preforms at low pressures, enabling production by simple and low cost investment casting methods, the production of pores with good connectivity due to the efficient packing of the spherical beads and, due to their porous nature, their rapid dissolution in warm water, making the production of large components viable.

It was apparent from this study that infiltration of molten metal into the porous beads can occur, particularly at higher infiltration pressures. As it is unlikely that this metal within the pores is load bearing [3], it is unclear as to what effect this might have on their mechanical response. As an extension to this previous work, this paper presents the structure and compressive mechanical properties for porous Al made by the infiltration of preforms made from porous, spherical NaCl beads with sizes ranging from 0.5 to 3.1 mm in diameter.

2. Results and Discussion

Table 1 presents the sintered preform densities (representative of those in the mould prior to infiltration) where the scatter in the density, given as one standard deviation, is low showing good reproducibility of the compaction and sintering processes. The preform densities can, as expected, be seen to increase with increasing compaction pressure. The density also increases with decreasing bead size, most likely due to increased sintering shrinkage within the beads, associated with the finer NaCl powder used to make them, rather than increased neck formation between beads [8].

Table 1. Summary of the preform density data (in g/cm^3) and densities for the resultant porous Al samples.

Condition	Preform Density	Porous Al Density	Bulk Infiltration	Bead Infiltration
0.5–1.0 mm 32 MPa, 1 bar	1.32 ± 0.01	0.79 ± 0.03		None
0.5–1.0 mm 32 MPa, 2.5 bar		0.89 ± 0.04		Low
0.5–1.0 mm 39 MPa, 1 bar	1.54 ± 0.01	0.27 ± 0.02	Partial infiltration	None
0.5–1.0 mm 39 MPa, 2.5 bar		0.40 ± 0.06	Partial infiltration	High
0.5–1.0 mm 50 MPa, 1 bar	1.59 ± 0.03	0.25 ± 0.03	Partial infiltration	None
0.5–1.0 mm 50 MPa, 2.5 bar		0.27 ± 0.03	Partial infiltration	High
1.4–2.0 mm 32 MPa, 1 bar	1.28 ± 0.02	0.71 ± 0.05		Low
1.4–2.0 mm 32 MPa, 2.5 bar		0.80 ± 0.01		Medium
1.4–2.0 mm 39 MPa, 1 bar	1.45 ± 0.01	0.41 ± 0.04		None
1.4–2.0 mm 39 MPa, 2.5 bar		0.56 ± 0.01		Medium
1.4–2.0 mm 50 MPa, 1 bar	1.55 ± 0.03	0.23 ± 0.04	Partial infiltration	None
1.4–2.0 mm 50 MPa, 2.5 bar		0.49 ± 0.02	Partial infiltration	High
2.5–3.1 mm 32 MPa, 1 bar	1.26 ± 0.01	0.53 ± 0.02		Medium
2.5–3.1 mm 32 MPa, 2.5 bar		0.67 ± 0.06		High
2.5–3.1 mm 39 MPa, 1 bar	1.44 ± 0.03	0.33 ± 0.03		Medium
2.5–3.1 mm 39 MPa, 2.5 bar		0.53 ± 0.02		High
2.5–3.1 mm 50 MPa, 1 bar	1.53 ± 0.04	0.15 ± 0.02	Partial infiltration	None
2.5–3.1 mm 50 MPa, 2.5 bar		0.45 ± 0.02	Partial infiltration	High

Examples of typical porous Al structures are presented in Figure 1 where the replication of different bead sizes is apparent. Table 1 also presents the densities of the porous Al structures and, as expected, the density increases with increasing infiltration pressure and decreasing preform density. For a number of samples, in particular those with high preform densities (approximately 1.53 g/cc and above) only partial infiltration took place. Owing to the inhomogenous nature of uni-axial compaction, it is expected that the high density compacts are comprised of regions which are of such high density that any porosity within them is no longer interconnected and cannot be infiltrated at any applied pressure and other regions that can, resulting in partial infiltration. It should be noted, however, that partial infiltration could be caused by premature freezing of the infiltrant since infiltration is not performed isothermally; the mould is initially below the melting point of the infiltrant and continually cooling. This is more likely for slow infiltration speeds at low infiltration pressures and into fine

channels with high surface area to volume ratios (which is the case for high compaction densities and small bead sizes).

Figure 1. X-ray tomographic images of foams made from (left to right) 0.5–1.0, 1.4–2.0 and 2.5–3.1 mm beads compacted at 32 MPa.

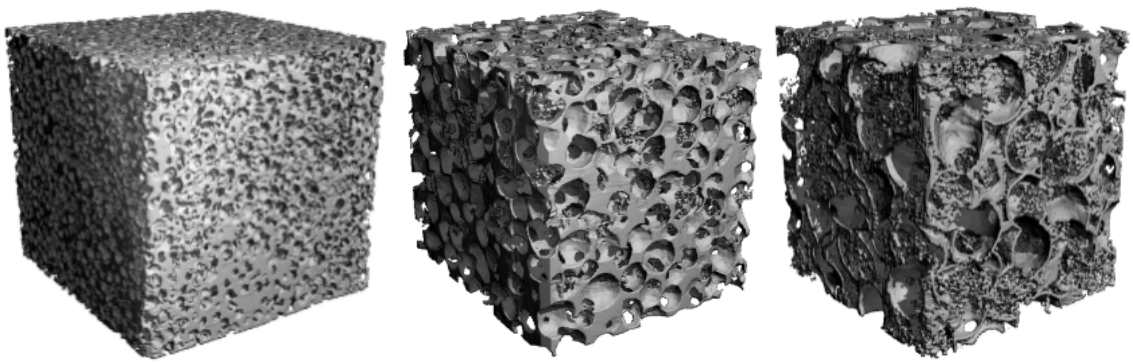

Figures 2–4 show SEM images of porous structures produced by infiltrating preforms made from 0.5–1.0, 1.4–2.0 and 2.5–3.1 mm beads respectively. In general, preforms pressed at 32 MPa contain a high fraction of porosity, with large channels, and this porosity is filled, even at low infiltration pressures, to give accurate replication of the round beads and an interconnected structure with thick cell walls. Small windows between neighbouring cells are observed, originating from the contact areas between salt spheres, magnified by the inability to fully infiltrate metal into the small gaps between these contacting particles. The struts are triangular in section, in keeping with preforms made by pressing rather than sintering. As the sintering shrinkage, and in particular the extent of neck formation, is small for these preforms made from relatively large aggregate beads, this is to be expected. For preforms compacted at 39, and in particular 50 MPa, many of the cell struts are incomplete, agreeing with the postulate for the formation of isolated Al struts for preforms with low relative densities [9,10].

For many of the porous structures, flow into porosity within the salt beads takes place, evidenced by fine nodular clusters within the pores. This is particularly evident for structures made with large beads, made from large salt particles, where significant infiltration into the beads can occur even at the lower infiltration pressure. Table 1 indicates to what approximate extent the beads themselves have been infiltrated. For many samples, the density for the porous structure made by infiltration at high pressure is much higher than that made at low pressure, despite the relatively small difference in infiltration pressure. From observations of the structure, it is apparent that the density increase is affected not by a significant increase in the thickness of the cell walls or connectivity of the cells, but by a higher fraction of metal being infiltrated into the porosity within the beads

Figure 2. SEM images of infiltration in 0.5–1.0 mm bead preforms compacted at (**a**) 32 MPa; (**b**) 39 MPa; and (**c**) 50 MPa at 1 bar; and (**d**) 32 MPa; (**e**) 39 MPa and (**f**) 50 MPa at 2.5 bar.

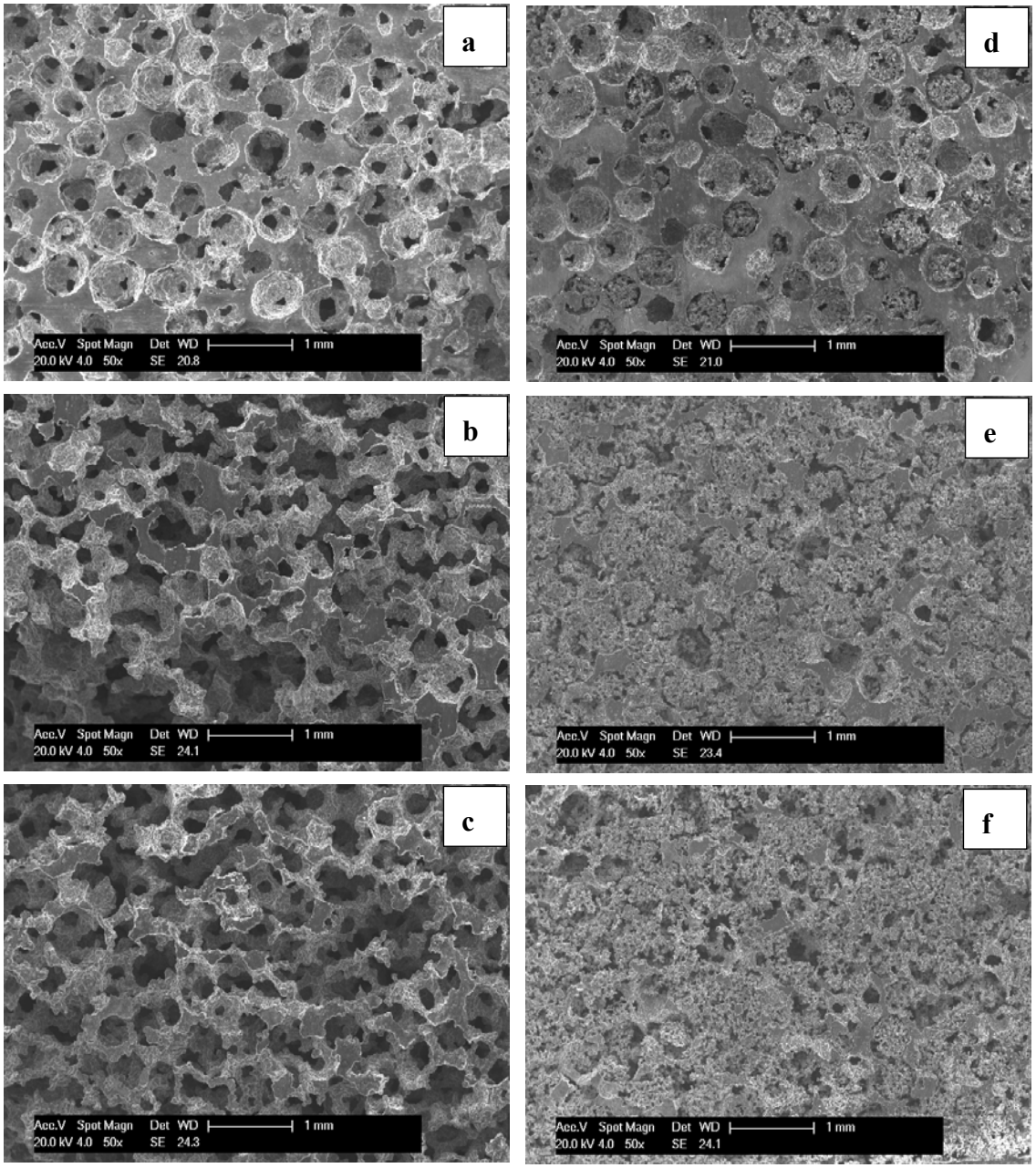

Figure 3. SEM images of infiltration in 1.4–2.0 mm bead preforms compacted at (**a**) 32 MPa; (**b**) 39 MPa; and (**c**) 50 MPa at 1 bar; and (**d**) 32 MPa; (**e**) 39 MPa and (**f**) 50 MPa at 2.5 bar.

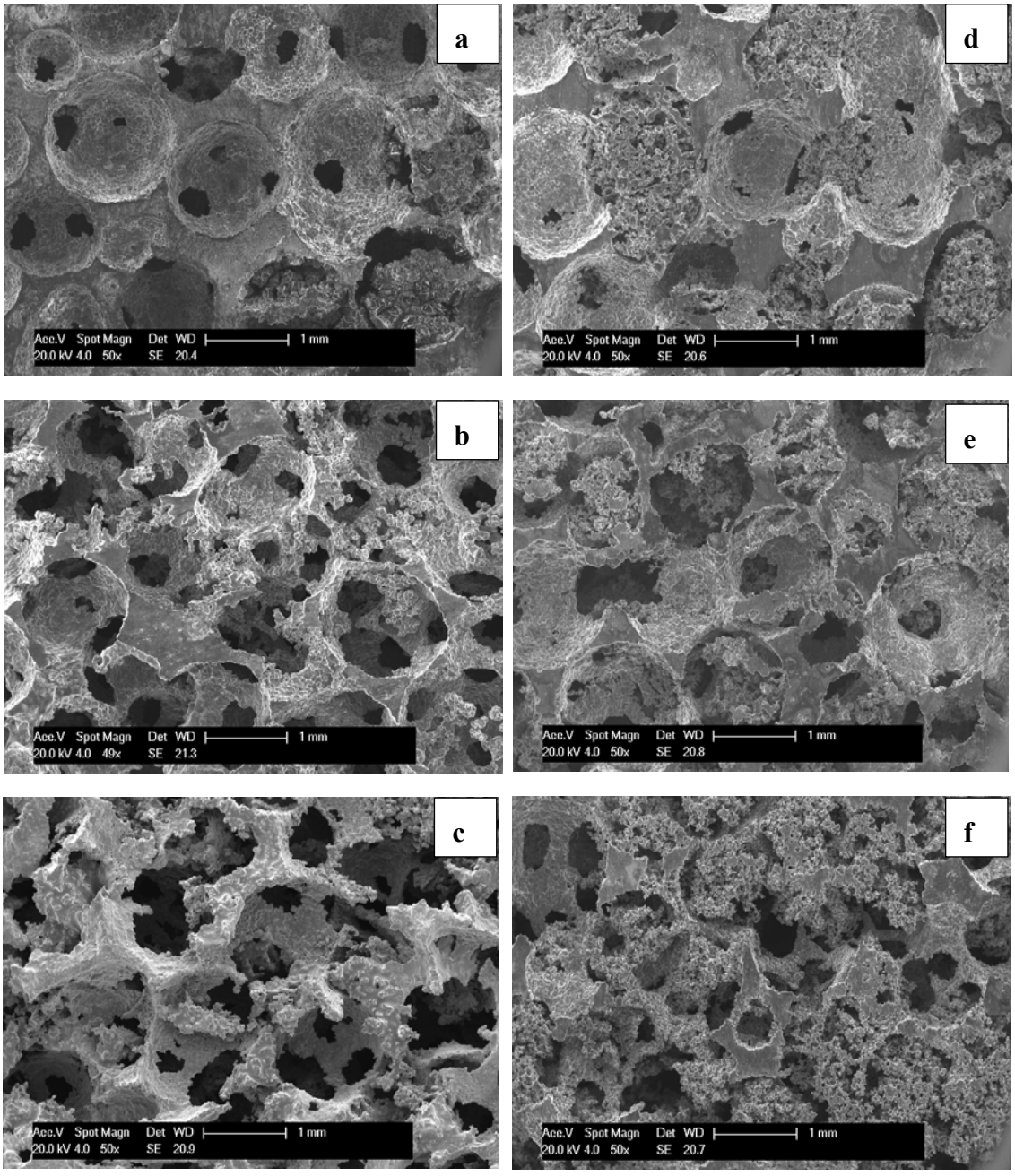

Figure 4. SEM images of infiltration in 2.5–3.1 mm bead preforms compacted at (**a**) 32 MPa; (**b**) 39 MPa; and (**c**) 50 MPa at 1 bar; and (**d**) 32 MPa; (**e**) 39 MPa and (**f**) 50 MPa at 2.5 bar.

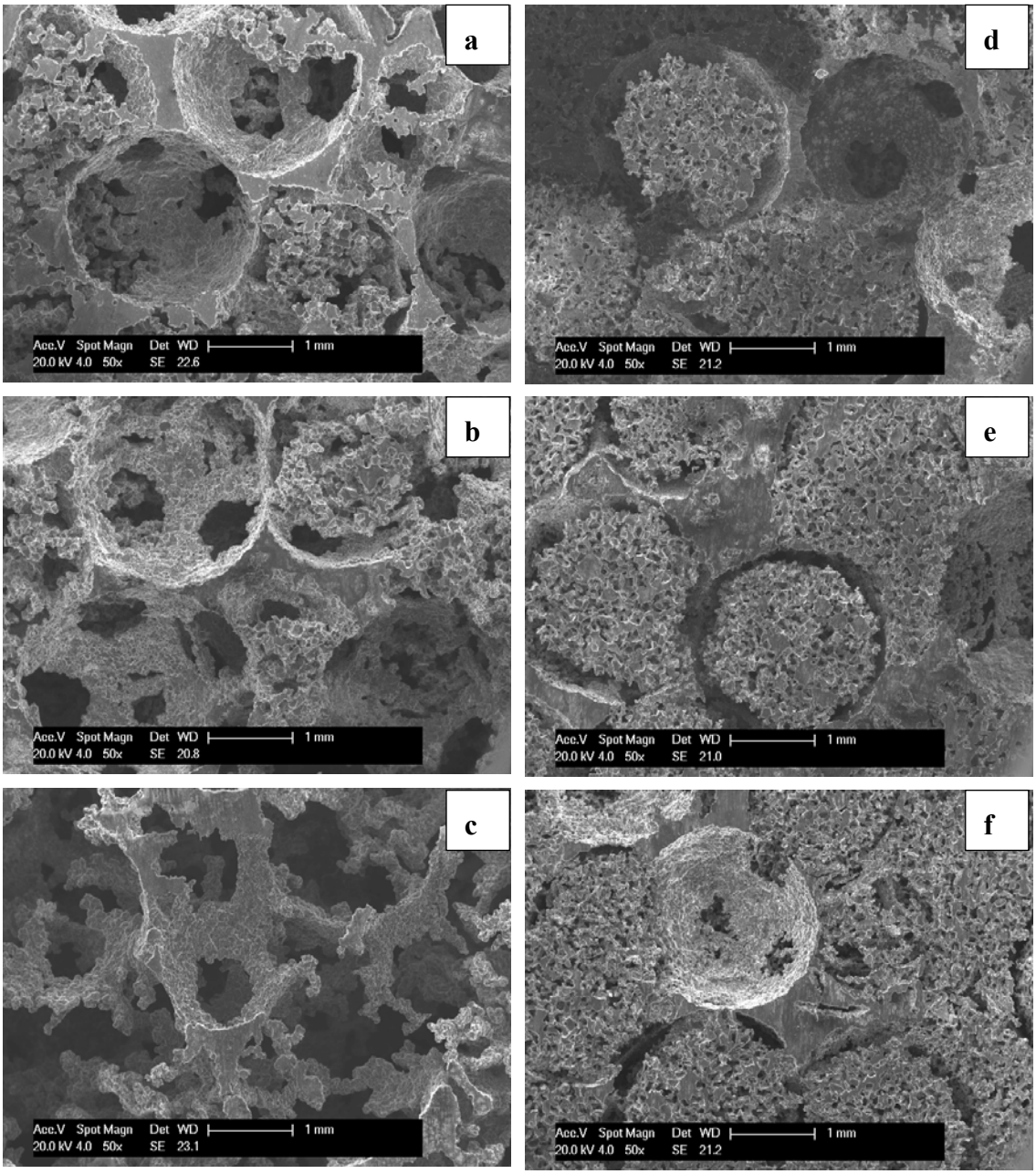

Infiltration of Al into the pores within the beads occurs in the same way as for the "bulk" of the preform and the extent depends upon the scale of the porosity in the beads, the applied pressure difference and the race to infiltrate before freezing takes place. Bead microstructures are shown in Figure 5, from which an increase in the scale of the intra-bead porosity with increasing bead size is apparent, as is their complex morphology which shows a relatively dense surface and large volumes of large interconnected pores (facets of the manufacturing process used to make them [6]). Previous work by these authors [6,7,11] quantified the pore structure within sintered beads using mercury porosimetry, showing the commencement of significant intrusion of mercury into the beads at pressures corresponding to pores sizes of approximately 15, 20 and 30 μm for 0.5–1.0, 1.4–2.0 and

2.5–3.1 mm beads respectively. Bead infiltration occurs by penetration of liquid through the fine surface pores and then becomes widespread throughout the large pores within the bulk of the bead with little additional increase in infiltration pressure. This accounts for the large increase in density for a relatively small increase in infiltration pressure. Evidence for infiltration in this way is also provided by the observation of gaps between the cell walls and the nodules (which is particularly clear in Figure 4d–f) created by limited infiltration through the dense bead surfaces.

Figure 5. SEM images of cross sections of (**a**) 0.5–1.0 mm; (**b**) 1.4–2.0 mm and (**c**) and (**d**) 2.5–3.1 mm sintered beads.

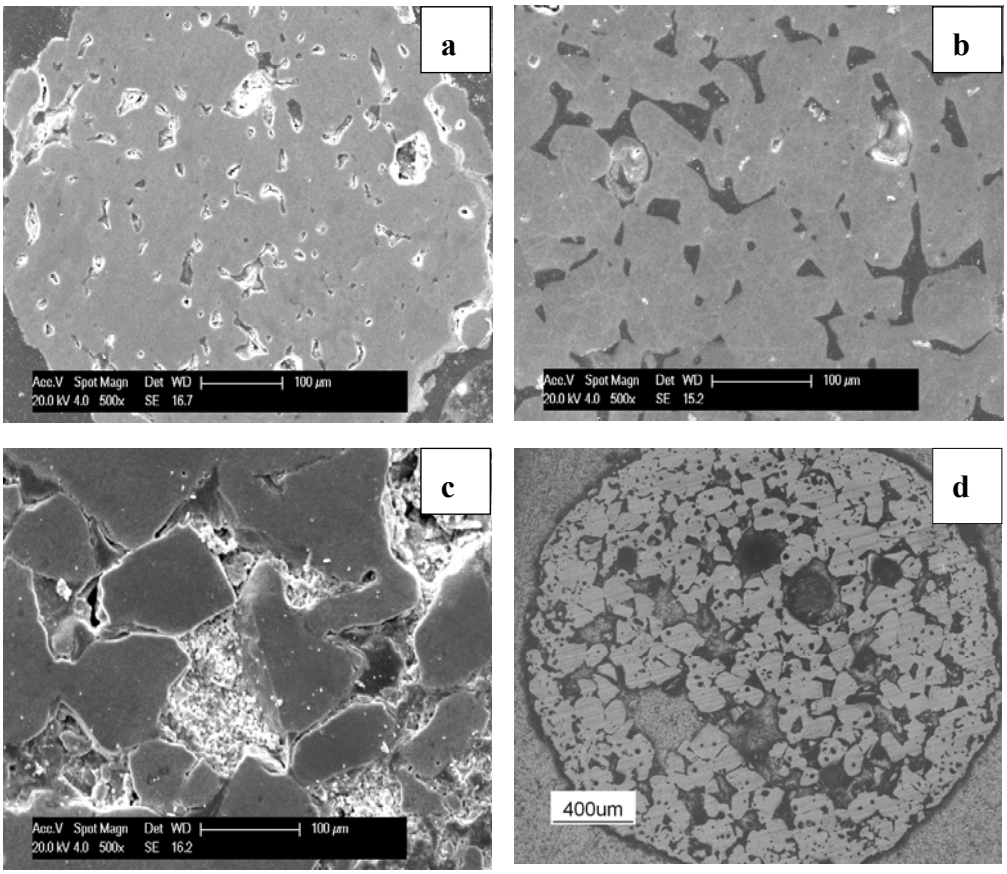

Infiltration of the beads can be predicted by considering the pressure required to infiltrate liquid into a single pore, as determined by the Young-Laplace equation;

$$P = \frac{2\sigma_{LV}\cos\theta}{r_h} \quad (1)$$

where P is the applied pressure, r_h is the pore radius, θ is the contact angle between the liquid and the solid and σ is the liquid-vapour (surface) tension. From measurements of the permeability of salt bead preforms with pure Al [7] the numerator in Equation 1 was be estimated to be −1.54. Pressures of 1 and 2.5 bar are, therefore, expected to infiltrate pores with diameters of approximately 30 and 12 μm respectively. These predictions agree well with observations of infiltration into all beads at high pressure and significant infiltration of large beads even at low pressures. The agreement is not absolute as the pore geometry is simplified and bead cracking and pore closure, especially at the surface of the bead, may occur during compaction.

Figure 6 presents compressive stress-strain curves for porous Al structures (that were fully infiltrated) made from different bead sizes. In general the σ–ε behaviour follows the expected trend, that the yield and plateau stress increase with increasing density. Table 2 presents the relative densities and relative 0.2% proof strengths and these data are also plotted on logarithmic axes in Figure 7. The relative yield strength was calculated assuming the 0.2% proof stress of pure aluminium to be 30 MPa for an alloy of 99.6% purity [12]) and the density of aluminium to be 2.7 g/cc. The standard deviation in the strength values presented in Table 2 shows that the properties are very reproducible and this is to be expected as the replication method using space holders (and the process used to make the salt beads) results in repeatable, uniform structures.

Figure 6. Compressive stress-strain curves for porous Al made from different beads, (**a**) 0.5–1.0 mm; (**b**) 1.4–2.0 mm; and (**c**) 2.5–3.1 mm.

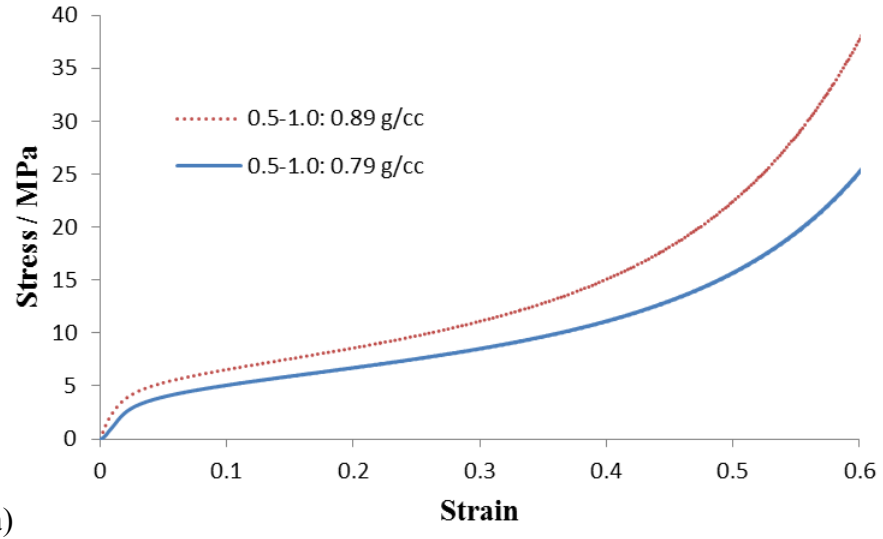

(**a**)

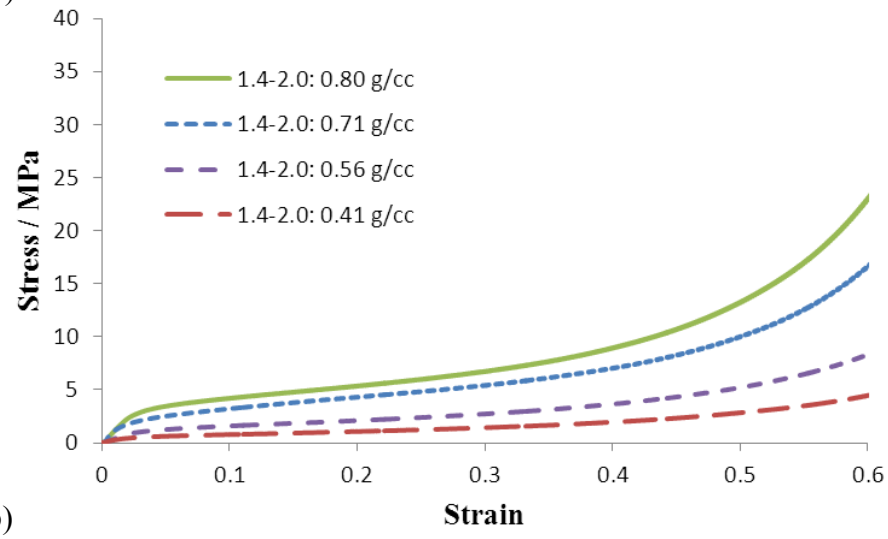

(**b**)

Figure 6. *Cont.*

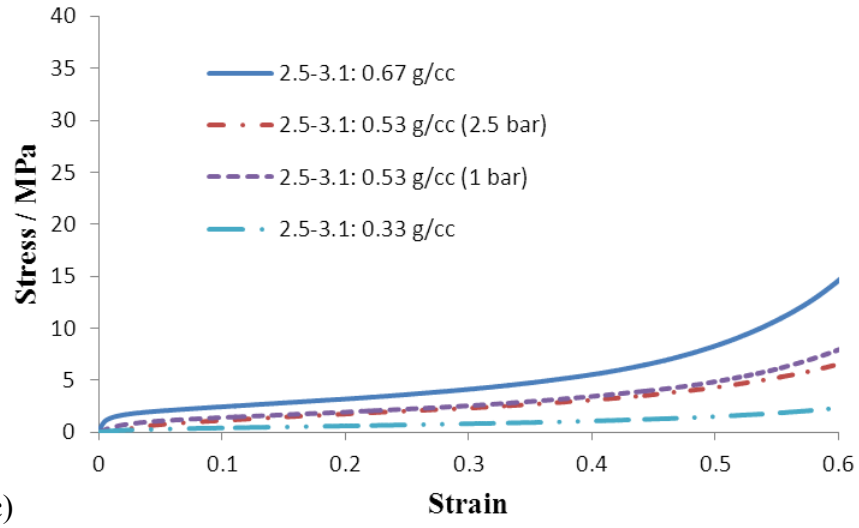

(c)

Table 2. Relative densities and relative 0.2% proof strengths for foams made from different bead sizes and preform compaction and infiltration pressures.

Condition	Relative density	Relative 0.2% proof strength	Dissolution time/min
0.5–1.0 mm 32 MPa, 1 bar	0.29	0.150 ± 0.01	60
0.5–1.0 mm 32 MPa, 2.5 bar	0.33	0.170 ± 0.01	90
1.4–2.0 mm 32 MPa, 1 bar	0.26	0.080 ± 0.01	45
1.4–2.0 mm 32 MPa, 2.5 bar	0.30	0.130 ± 0.01	60
1.4–2.0 mm 39 MPa, 1 bar	0.15	0.022 ± 0.002	30
1.4–2.0 mm 39 MPa, 2.5 bar	0.21	0.072 ± 0.001	45
2.5–3.1 mm 32 MPa, 1 bar	0.20	0.047 ± 0.004	30
2.5–3.1 mm 32 MPa, 2.5 bar	0.26	0.059 ± 0.005	45
2.5–3.1 mm 39 MPa, 1 bar	0.13	0.009 ± 0.001	15
2.5–3.1 mm 39 MPa, 2.5 bar	0.20	0.038 ± 0.001	30

The 0.2% proof strengths for the porous Al foams (ranging from 0.27 MPa at a metal fraction of 0.13, to 5.1 MPa at a metal fraction of 0.33) are as much as 3 times higher than those measured for similar pure Al foams made in the same way [2,3], but this difference is likely to be due to the effect of compositional differences on the yield stress of the bulk metal (for example the yield stress of Al varies between 10 MPa for 99.99% and 30 MPa for 99.6% purity [12]).

There are a number of instances where porous structures with different pore sizes, but similar densities, enable the influence of pore size to be assessed. For porous structures with relative densities of 0.3, 0.26 and 0.2, a decrease in pore size always leads to an increase in 0.2% proof stress. Whilst this might, in part, be attributable to the increased strengthening effect of the oxide layer developed on the surfaces of smaller pores during leaching [5], this is less likely than the effect of differences in cellular structure. In all cases, the porous metal with the smaller pore size was manufactured at low infiltration pressure, resulting in much less metal infiltration within the beads themselves. From a comparison of porous structures with the same bead size and density (32 MPa −1 bar and 39 MPa −2.5 bar, both with a relative density of 0.2) it is apparent that when a large fraction of the metal is

distributed within the pores, due to infiltration within the beads at the higher infiltration pressure, the proportion of metal in the load-bearing cellular structure is reduced and the yield strength is lower.

The plastic collapse, or yield stress can be related to the relative foam density using Equation 2. In this equation, σ_{ys} is the yield (or proof) stress of the cell wall material, ρ^* is the density of the porous metal and ρ_s that for the bulk (cell wall) material, C is a constant and n for an open cell structure, where the struts are assumed to be straight, thin beams with perfect plasticity, is 1.5. Previous studies have shown typical values for n for replicated pure aluminium foams with relative densities above 0.13, to be in the range of 2.3–2.7 [13–15], increasing to as high as 3.7 for porous metals with very low relative densities [16]. The large deviation from the model is attributed to the struts in the "real" porous structures resembling plates, which are thinner at the middle, and them being much less efficient at strengthening the porous structure.

$$\frac{\sigma_{pl}}{\sigma_{ys}} = C\left(\frac{\rho^*}{\rho_s}\right)^n \quad (2)$$

When the exponent n is calculated from the slope of the best-fit line in Figure 7, a value of 2.9 is obtained. If the data are split into those for infiltration at low pressure and those at high pressure, where a larger proportion of the bead is infiltrated and a significant fraction of metal lies within the cells, values of 2.8 and 3.1 are obtained, respectively, indicating a more efficient structure for infiltration at low pressure, supporting the compression data.

Figure 7. Log-log plot of relative proof stress and relative density.

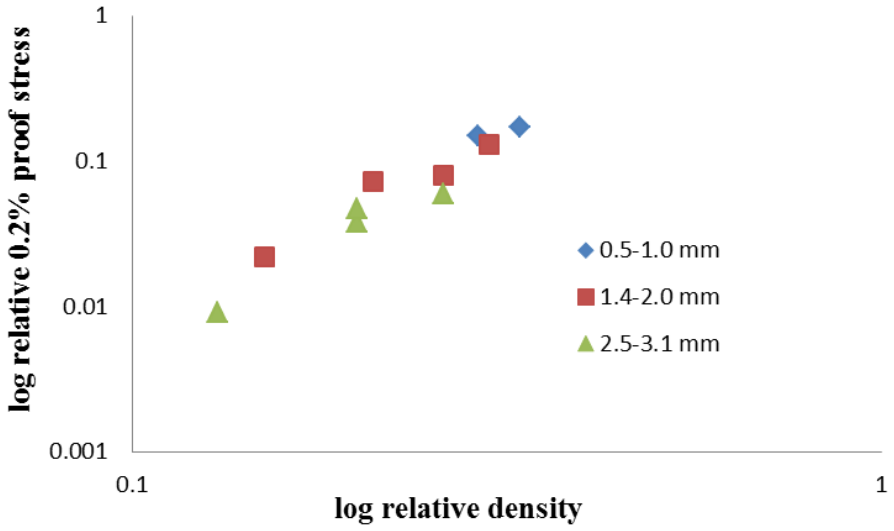

Table 2 also compares the dissolution behaviour for the different precursors. In general, the dissolution time decreases as the bead size and compaction pressure increase. Higher compaction pressures result in increased connectivity of the salt bead structure (both in terms of the co-ordination number and the contact area [17]) and larger beads lead to larger channels, allowing easier ingress of water and egress of NaCl and increased rates of dissolution. Infiltrating the preform at higher pressure results in an increase in the time required to remove the NaCl. This is partly due to the decreased connectivity of the salt in the structure, but also due to the extensive infiltration of metal within the salt beads, creating an additional network of interpenetrating fine channels of metal and salt. It should be

remarked, however, that due to the porous nature of the beads, salt removal is rapid compared with monolithic salt of a similar size (taking 240 min for 0.3–1.5 mm salt to be removed in hot water at 95 °C [18]) due to the ability of for the porous beads to collapse as well as dissolve.

3. Experimental Section

Porous salt beads with sizes between 0.5–1.0, 1.4–2.0 and 2.5–3.1 mm were made by a process detailed in [6,11] involving the disintegration of a paste containing pre-gelatinised flour, water and NaCl powder, in oil. In order to make smaller beads, the intensity of the shearing used to disintegrate the paste was increased. Additionally, finer NaCl powder was used, with <53 μm, 53–106 μm and 106–180 μm NaCl powder being used for the 0.5–1.0 mm, 1.4–2.0 and 2.5–3.1 mm beads respectively.

To make preforms for subsequent infiltration, the beads were poured into a 22 mm diameter steel die, tapped a few times to improve packing and then uni-axially compacted at pressures of either 32, 39 or 50 MPa. The densities of the preforms after sintering at 730 °C for 4 h (typical of their condition prior to infiltration), were measured from their geometry and their mass.

Foams were produced by a pressure-assisted vacuum investment casting process detailed in [7], using an Indutherm VC 400 machine. The flask mould, containing the preforms, was preheated in a separate oven, first to 730 °C for 4 hours to cure the investment, then cooled to the casting temperature of 600 °C, before being loaded into the lower chamber. The 99.5% pure Al charge was poured at 760 °C and infiltration was conducted with the mould under vacuum, a pressure difference of approximately 1 bar (equivalent to 0.1 MPa) and also with an additional 1.5 bar nitrogen gas over-pressure (a pressure difference of approximately 2.5 bar, 0.25 MPa). Gas pressure and vacuum were maintained whilst cooling and solidification took place, after which the flask was removed and quenched into cold water to disintegrate the investment and retrieve the casting. A minimum of 9 preforms were infiltrated for each preform and pressure condition.

Samples with square cross sections were machined from the infiltrated preforms to dimensions of 14 × 14 mm, 18 mm high. Salt removal was affected by their immersion in static water, at 65 °C and for NaCl dissolution tests, the samples were removed, dried and weighed every 15 min. The time to remove >99% of the salt was reported as the dissolution time. After complete NaCl removal, the density was determined from the mass and volume of the sample. The porous structures were characterised using X-ray computed tomography (Scanco AG, μCT40), optical microscopy and scanning electron microscopy (SEM).

Samples were compression tested using an Instron machine with a 5kN load cell at a cross head speed, of 1.8 mm/min. The 0.2% proof stress was measured for a minimum of five samples per condition. Although the dimensions for the compression test samples are relatively small compared with the largest pore sizes, they are compliant with testing standards (JIS H 7902, September 2008; requires the minimum dimensions to be >4 times the maximum pore size or >7 times the average pore size). Whilst it is acknowledged that test samples with the largest pore sizes do not meet the later condition, it is unlikely that any strength variations observed between pores sizes (especially for the smaller two bead sizes) will be due to the test sample size.

4. Conclusions

Preforms made from porous salt beads with different diameters (0.5–1.0, 1.4–2.0 and 2.5–3.1 mm) have been infiltrated with molten Al to produce porous structures using pressure-assisted vacuum investment casting. Infiltration was incomplete for preforms with high densities. At higher infiltration pressures, penetration of molten Al occurred into beads of all sizes. The infiltration behaviour within the beads was predicted using a simple model.

The yield strength of the porous structures increased with increasing density and decreasing pore (bead) size. Despite the non-optimum distribution of metal in the porous structure, due to partial infiltration within the beads, the magnitude and density dependence of the yield stress were comparable with those for pure Al foams reported in similar studies. The structural efficiency was improved for structures produced at lower infiltration pressure, where the metal is predominantly distributed in the cell walls.

The rate of salt dissolution from the preforms was high, in particular for high density preforms, large beads and preforms infiltrated at low pressures, owing to the ability of the porous beads to collapse as well as dissolve.

Acknowledgments

Appichart Jinnapat would like to thank the Royal Thai Air Force for financial support.

References

1 Sun, D.; Zhao, Y. Static and dynamic energy absorption of Al foams produced by the sintering and dissolution process. *Metal. Mater. Trans. B* **2003**, *34*, 69–74.

2 Goodall, R.; Despois, J.F.; Marmottant, A.; Salvo, L.; Mortensen, A. The effect of preform processing on replicated aluminium foam structure and mechanical properties. *Scripta Mater.* **2006**, *54*, 2069–2073.

3 Goodall, R.; Marmottant, A.; Salvo, L.; Mortensen, A. Spherical pore replicated microcellular aluminium: Processing and influence on properties. *Mater. Sci. Eng. A* **2007**, *465*, 124–135.

4 Goodall, R.; Mortensen, A. Microcellular aluminium: Child's play. *Adv. Eng. Mater.* **2007**, *9*, 951–954.

5 Diologent, F.; Goodall, R.; Mortensen, A. Surface oxide in replicated microcellular aluminium and its influence on the plasticity size effect. *Acta Mater.* **2009**, *57*, 286–294.

6 Jinnapat, A.; Kennedy, A.R. The manufacture of spherical salt beads and their use as dissolvable templates for the production of cellular solids via a powder metallurgy route. *J. Alloys Compd.* **2010**, *499*, 43–47.

7 Jinnapat, A.; Kennedy, A.R. The manufacture and characterization of aluminum foams made by investment casting using dissolvable spherical sodium chloride bead performs. *Metals* **2011**, *1*, 49–64.

8 Goodall, R.; Despois, J.F.; Mortensen, A. Sintering of NaCl powder: Mechanisms and first stage kinetics. *J. Eur. Ceram. Soc.* **2006**, *26*, 3487–3497.

9 Hao, G.; Han, F.; Li, W. Processing and mechanical properties of magnesium foams. *J. Porous Mater.* **2009**, *16*, 251–256.
10 Zhao, Y.Y.; Sun, D.X. A novel sintering-dissolution process for manufacturing Al foams. *Scripta Mater.* **2001**, *44*, 105–110.
11 Jinnapat, A. The Manufacture and Characterisation of Aluminium Foams Made by Investment Casting Using Dissolvable Spherical Sodium Chloride Bead Performs. Ph.D. Thesis. University of Nottingham, Nottingham, UK, September 2011.
12 Hatch, J.E. *Aluminum: Properties and Physical Metallurgy*; Aluminum Association Inc. and ASM International: Metals Park, OH, USA, 1984.
13 San Marchi, C.; Mortensen, A. Deformation of open-cell aluminum foam. *Acta Mater.* **2001**, *49*, 3959–3969.
14 Despois, J.-F.; Mueller, R.; Mortensen, A. Uniaxial deformation of microcellular metals. *Acta Mater.* **2006**, *54*, 4129–4142.
15 Diologent, F.; Combaz, E.; Laporte, V.; Goodall, R.; Weber, L.; Duc, F.; Mortensen, A. Processing of Ag-Cu alloy foam by the replication process. *Scripta Mater.* **2009**, *61*, 351–354.
16 Amsterdam, E.; Goodall, R.; Mortensen, A.; Onck, P.R.; de Hosson, J.T.M. Fracture behavior of low-density replicated aluminum alloy foams. *Mater. Sci. Eng. A* **2008**, *496*, 376–382.
17 Marmottant, A.; Salvo, L.; Martin, C.L.; Mortensen, A. Coordination measurements in compacted NaCl irregular powders using X-ray microtomography. *J. Eur. Ceram. Soc.* **2008**, *28*, 2441–2449.
18 Zhao, Y.; Han, F.; Fung, T. Optimisation of compaction and liquid-state sintering in sintering and dissolution process for manufacturing Al foams. *Mater. Sci. Eng. A* **2004**, *364*, 117–125.